

## Supporting Information

### **New Deep Hole-Trapping Site for Water Splitting on Rutile TiO<sub>2</sub>(110) Surface**

He Zhou, Xiao Zhang, Jie Zhang, Huizhong Ma, Fan Jin and Yuchen Ma\*

School of Chemistry and Chemical Engineering, Shandong University, Jinan, China

\* E-mail: myc@sdu.edu.cn

## Validity to use DFT-PBE in geometry optimization for OER

DFT is the most popular approach applied in theoretical studies on  $\text{TiO}_2$ . However, it is still an open question which level of DFT (GGA/LDA, DFT+U or hybrid DFT) is more appropriate. Recent STM measurements demonstrate that the activation barrier for a  $\text{H}_2\text{O}$  molecule adsorbed at  $\text{Ti}_{5c}$  to transfer one H to an adjacent  $\text{O}_{br}$  (from state II to state III in Fig. 1 of the main context of this paper) is about  $0.1 \text{ eV}$ <sup>1</sup>. PBE predicts a similar barrier according to calculations by us in this work ( $0.14 \text{ eV}$  as shown in Fig. S1a) and by Hou *et al.* ( $0.22 \text{ eV}$ )<sup>1</sup>. In contrast, hybrid DFT at the level of HSE06 and DFT+U with  $U=6.3 \text{ eV}$  for O give too larger values ( $0.72 \text{ eV}$  and  $0.97 \text{ eV}$  respectively)<sup>2</sup>. We compare the electronic structures of some OER intermediates computed within PBE and DFT+U ( $U=4.0 \text{ eV}$  for Ti and  $6.0 \text{ eV}$  for O), as presented below. Overall, results from PBE are closer to those from GW.

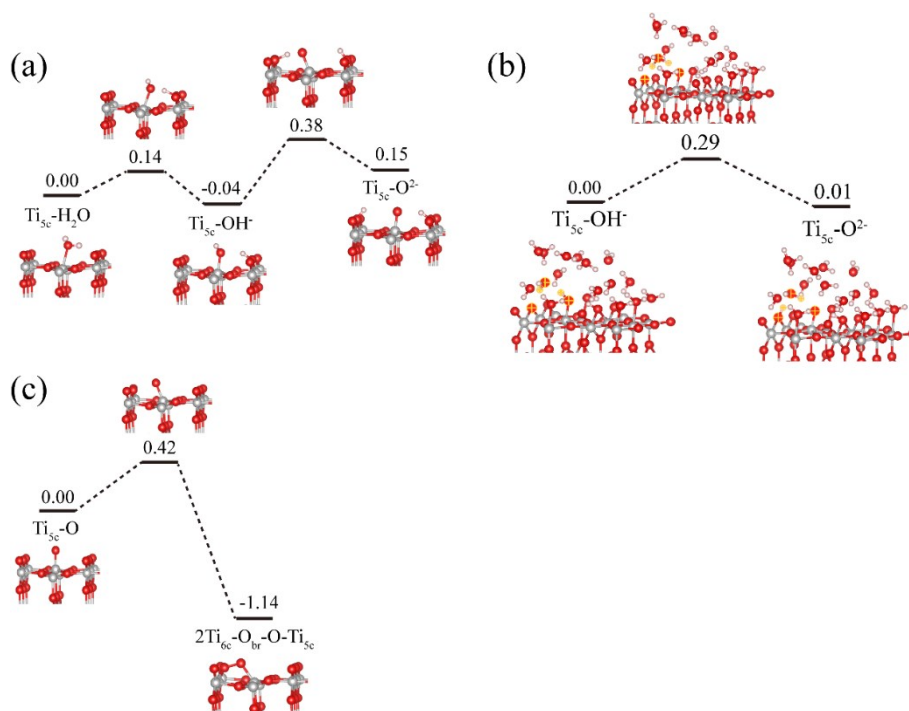


**Figure S1** Potential surfaces of some reactions. (a) Deprotonation of H<sub>2</sub>O adsorbed at Ti<sub>5c</sub> to Ti<sub>5c</sub>-OH<sup>-</sup> and then to Ti<sub>5c</sub>-O<sup>2-</sup> in vacuum. (b) Deprotonation of Ti<sub>5c</sub>-OH<sup>-</sup> to Ti<sub>5c</sub>-O<sup>2-</sup> in aqueous solution. (c) Transformation of Ti<sub>5c</sub>-O to 2Ti<sub>6c</sub>-O<sub>br</sub>-O-Ti<sub>5c</sub> in vacuum. (a) and (c) are computed by CI-NEB. In (b), a H<sub>2</sub>O in aqueous solution participates in the proton transfer. All the O and H involved in the reaction are highlighted in (b). The potential surface in (b) is computed by fixing positions of O in Ti<sub>5c</sub>-OH<sup>-</sup> and O in the involved H<sub>2</sub>O, moving the H between these two O by hand gradually, while all the other atoms except those of the bottom O-Ti-O trilayer are allowed to relax.

## 1. Electronic structures of $\text{Ti}_{5c}\text{-OH}^-$

From Fig. S2, onset of the O 2p level belonging to  $\text{Ti}_{5c}\text{-OH}^-$  lies in nearly the same position below VBM within GW, PBE and DFT+U. Since the spin-up and the spin-down states are symmetric in the DOS within PBE and DFT+U, non-spin-polarized GW calculation is used here to save the huge computational cost of GW.

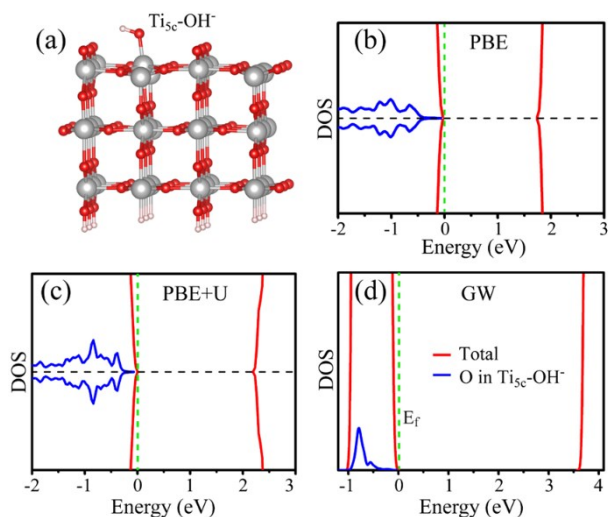


**Figure S2** (a) Geometry of  $\text{Ti}_{5c}\text{-OH}^-$ . (b), (c) and (d): Total (red lines) and projected (blue lines) DOSs computed by PBE, PBE+U ( $U=4.0$  eV for Ti and  $6.0$  eV for O) and GW for  $\text{Ti}_{5c}\text{-OH}^-$ . Green dashed lines mark the Fermi levels. The reference energy is set to VBM.

## 2. Electronic structures of $\text{Ti}_{5c}\text{-O}^{2-}$

From Fig. S3, distribution of the O 2p level belonging to  $\text{Ti}_{5c}\text{-O}^{2-}$  computed within PBE resembles that within GW, while the DFU+U result deviates a lot from GW. Since the spin-up and the spin-down states are symmetric in the DOS within PBE and DFT+U, non-spin-polarized GW calculation is used here to save the huge computational cost of GW.

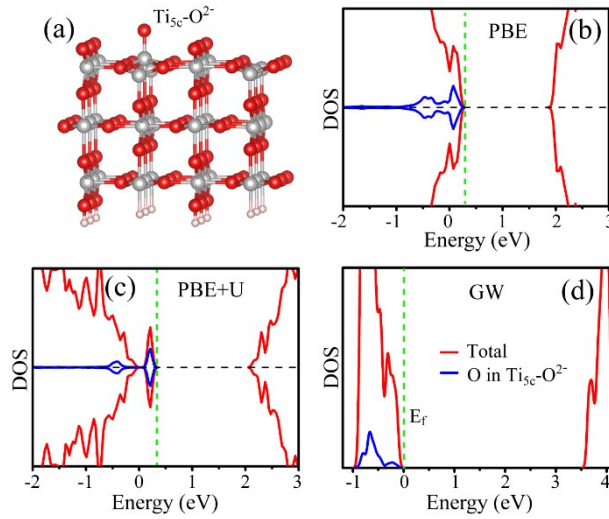


**Figure S3** (a) Geometry of  $\text{Ti}_{5c}\text{-O}^{2-}$ . (b), (c) and (d): Total (red lines) and projected (blue lines) DOSs computed by PBE, PBE+U ( $U=4.0$  eV for Ti and  $6.0$  eV for O) and GW for  $\text{Ti}_{5c}\text{-O}^{2-}$ . Green dashed lines mark the Fermi levels. The reference energy is set to VBM.

### 3. Electronic structures of $\text{Ti}_{5c}\text{-O}^-$

From Fig. S4, the lowest unoccupied molecular orbital (LUMO) is 0.1 eV above VBM in PBE. In DFT+U, LUMO lies 2.2 eV above VBM, very close to CBM. In GW, LUMO is 0.8 eV above VBM. Spin-polarized GW calculation is performed here. The GW DOS presented in Fig. S4d below is the sum of spin-up and spin-down channels. Distribution of LUMO in PBE (Fig. S4e) and LDA (Fig. S4g) resembles that computed by osscGW (Fig. S4f).

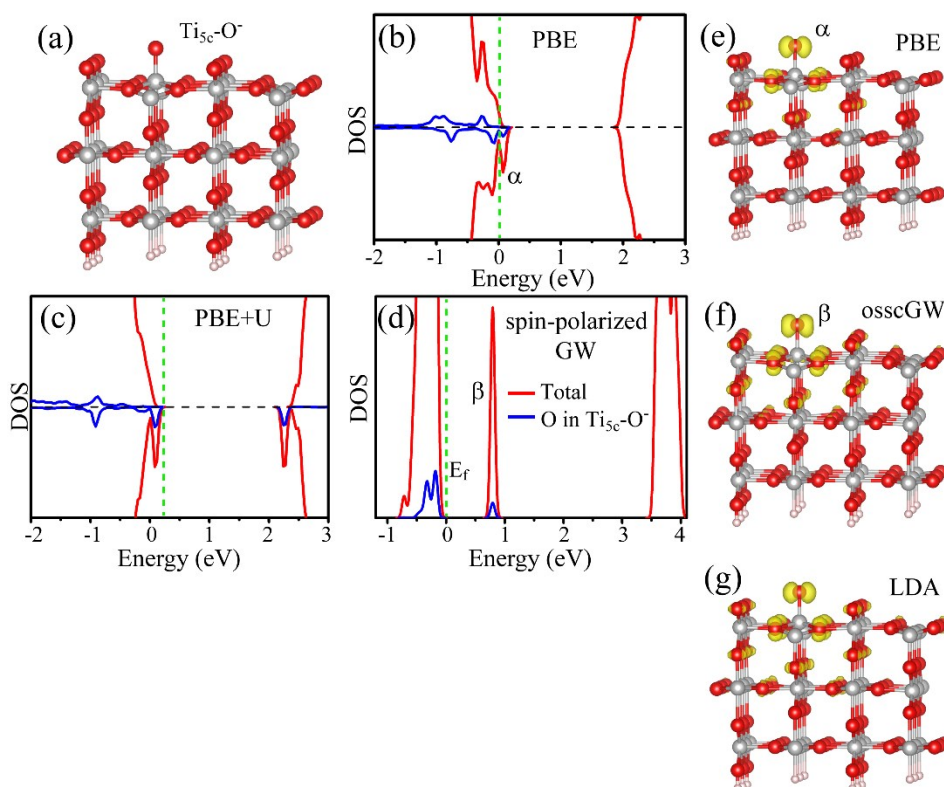


**Figure S4** (a) Geometry of  $\text{Ti}_{5c}\text{-O}^-$ . (b), (c) and (d): Total (red lines) and projected (blue lines) DOSs computed by PBE, PBE+U ( $U=4.0$  eV for Ti and  $6.0$  eV for O) and GW for  $\text{Ti}_{5c}\text{-O}^-$ . Green dashed lines mark the Fermi levels. The reference energy is set to VBM. GW DOS in (d) is the sum of spin-up and spin-down channels. (e), (f): Spatial distributions of the states  $\alpha$  and  $\beta$ , as marked in (b) and (d), computed within PBE and osscGW respectively. (g) Spatial distribution of the in-gap LUMO computed within LDA.

#### 4. Electronic structures of $\text{Ti}_{5c}\text{-O}$

In PBE, the triplet state of  $\text{Ti}_{5c}\text{-O}$  is 0.02 eV more stable than its singlet state. In this work we only study its singlet state due to three reasons. Firstly, ground state of its successor,  $2\text{Ti}_{6c}\text{-O}_{br}\text{-O-Ti}_{5c}$ , is a singlet; transformation from  $\text{Ti}_{5c}\text{-O}$  to  $2\text{Ti}_{6c}\text{-O}_{br}\text{-O-Ti}_{5c}$  is allowed only when  $\text{Ti}_{5c}\text{-O}$  stays in its singlet state. Secondly, energy difference between the singlet and the triplet states of  $\text{Ti}_{5c}\text{-O}$  is minor; environmental effects, including aqueous solution, defects and other surface groups around, might convert the energy sequence between singlet and triplet states. Thirdly, in principle current GW method cannot treat open-shell systems. Luckily, the DOSs in spin-polarized and non-spin-polarized PBE (Fig. S5b and Fig. S5d) exhibit similar features. In both cases, positions of the in-gap empty states, which are mostly concerned in this work, are similar. In non-spin-polarized GW (Fig. S5e), the in-gap empty state locates 0.8 eV above VBM. This is consistent with position of the in-gap empty state of  $\text{Ti}_{5c}\text{-O}$  computed by spin-polarized GW (Fig. S4d). In Fig. S5c, for comparison we still try to give a spin-polarized GW DOS based on the triplet ground-state electronic structure, although this GW DOS may be not very accurate since the current GW method cannot treat open-shell triplet states. Comparing to Fig. S5e, the in-gap empty states in Fig. S5c downshift to VBM a little bit. However, this does not influence the conclusions in our work.

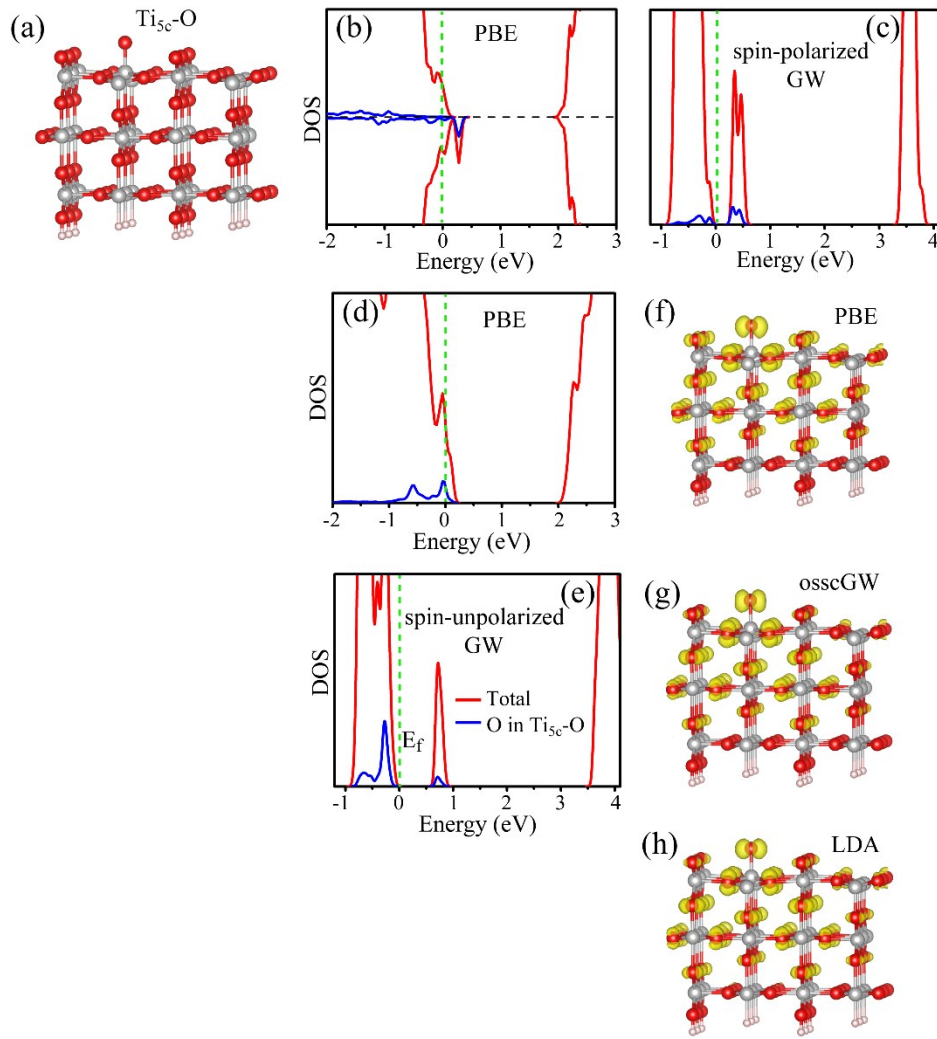


**Figure S5** (a) Geometry of  $\text{Ti}_{5c}\text{-O}$ . (b), (c), (d) and (e): Total (red lines) and projected (blue lines) DOSs computed by spin-polarized PBE, spin-polarized GW, spin-unpolarized PBE and spin-unpolarized GW for  $\text{Ti}_{5c}\text{-O}$ . GW DOS in (c) is the sum of spin-up and spin-down channels. Green dashed lines mark the Fermi levels. The reference energy is set to VBM. (f) Spatial distributions of the in-gap empty state in (d) computed within PBE. (g) Spatial distribution of the in-gap empty state in (e) computed within osscGW. (h) Spatial distribution of the in-gap empty state computed within LDA. It can be seen that PBE, LDA and osscGW give similar spatial distribution for the hole state.

## 5. Electronic structures of $2\text{Ti}_{6c}\text{-O}_{br}\text{-O-Ti}_{5c}$

The ground state of  $2\text{Ti}_{6c}\text{-O}_{br}\text{-O-Ti}_{5c}$  is a singlet in both PBE and DFT+U (Fig. S6). The DOS in PBE is nearly symmetric for the spin-up and spin-down channels. So GW calculation is carried out without the consideration of spin polarization to save the huge computational cost of GW. Both PBE and DFT+U reproduce well energy positions of the in-gap occupied states calculated within GW. BSE calculations for the excited states shown in Fig. 3 of the main context are done without the consideration of spin polarization to save the huge computational cost of GW+BSE.

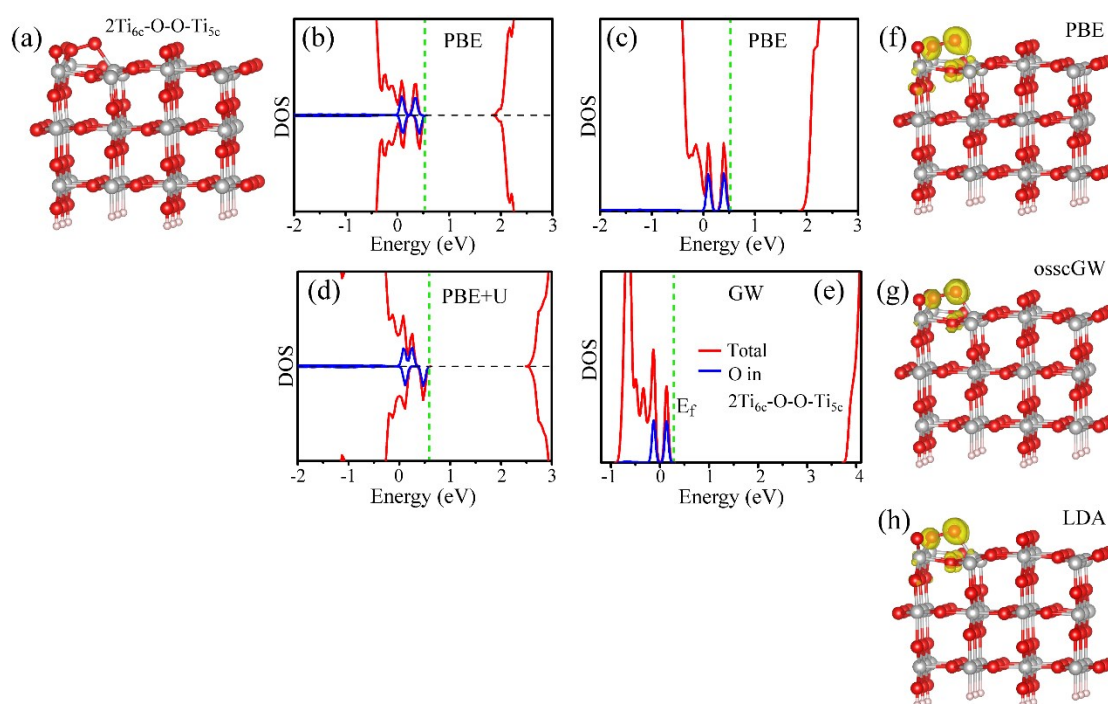


**Figure S6** (a) Geometry of  $2\text{Ti}_{6c}\text{-O}_{br}\text{-O-Ti}_{5c}$ . (b), (c), (d) and (e): Total (red lines) and projected (blue lines) DOSs computed by spin-polarized PBE, spin-unpolarized PBE, spin-polarized PBE+U ( $U=4.0$  eV for Ti and  $6.0$  eV for O) and spin-unpolarized GW for  $2\text{Ti}_{6c}\text{-O}_{br}\text{-O-Ti}_{5c}$ . Green dashed lines mark the Fermi levels. The reference energy is set to VBM. (f) Spatial distributions of HOMO in (c) computed within PBE. (g) Spatial distribution of HOMO in (e) computed within osscGW. (h) Spatial distribution of HOMO computed within LDA. It can be seen that PBE, LDA and osscGW give similar spatial distribution for HOMO.

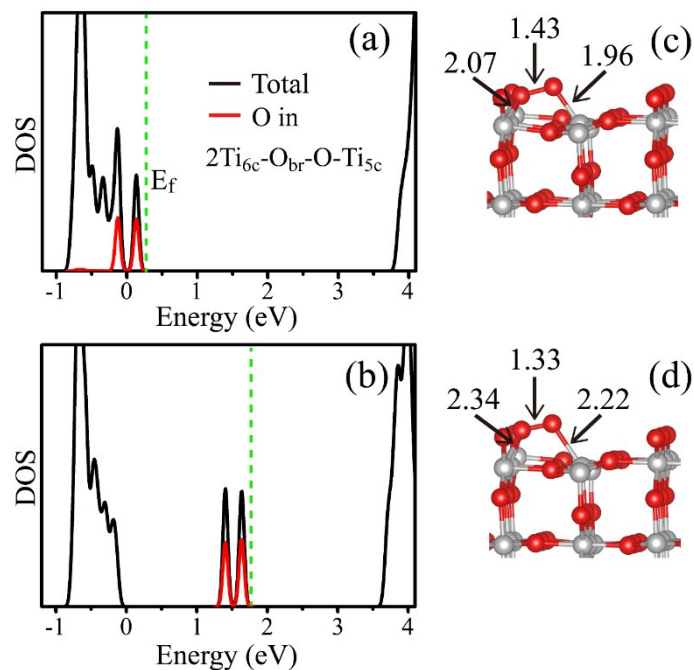


**Figure S7** (a) [(b)] Total (black line) and projected (red line) DOSs of  $2\text{Ti}_{6c}\text{-O}_{br}\text{-O-Ti}_{5c}$  in its ground-state equilibrium geometry as shown in (c) optimized by DFT [excited-state equilibrium geometry as shown in (d) optimized by CDFT]. Green dashed lines mark the Fermi levels. The reference energy is set to VBM.

- 1 S. Tan, H. Feng, Q. Zheng, X. Cui, J. Zhao, Y. Luo, J. Yang, B. Wang and J. G. Hou, *J. Am. Chem. Soc.*, 2020, **142**, 826-834.
- 2 D. Wang, T. Sheng, J. Chen, H.-F. Wang and P. Hu, *Nat. Catal.*, 2018, **1**, 291-299.